Tyrosine Residues Serve as Proton Donor in the Catalytic Mechanism of Epoxide Hydrolase from *Agrobacterium radiobacter*

Rick Rink, Jaap Kingma, Jeffrey H. Lutje Spelberg, and Dick B. Janssen*

Department of Biochemistry, Groningen Biomolecular Sciences and Biotechnology Institute, University of Groningen, Nijenborgh 4, 9747 AG, Groningen, The Netherlands

Received September 27, 1999; Revised Manuscript Received January 7, 2000

ABSTRACT: Epoxide hydrolase from *Agrobacterium radiobacter* catalyzes the hydrolysis of epoxides to their diols via an alkyl-enzyme intermediate. The recently solved X-ray structure of the enzyme shows that two tyrosine residues (Tyr152 and Tyr215) are positioned close to the nucleophile Asp107 in such a way that they can serve as proton donor in the alkylation reaction step. The role of these tyrosines, which are conserved in other epoxide hydrolases, was studied by site-directed mutagenesis. Mutation of Tyr215 to Phe and Ala and mutation of Tyr152 to Phe resulted in mutant enzymes of which the k_{cat} values were only 2−4-fold lower than for wild-type enzyme, whereas the K_m values for the (*R*)-enantiomers of styrene oxide and *p*-nitrostyrene oxide were 3 orders of magnitude higher than the K_m values of wild-type enzyme, showing that the alkylation half-reaction is severely affected by the mutations. Pre-steady-state analysis of the conversion of (*R*)-styrene oxide by the Y215F and Y215A mutants showed that the 1000-fold elevated K_m values were mainly caused by a 15−40-fold increase in K_S and a 20-fold reduction in the rate of alkylation. The rates of hydrolysis of the alkyl-enzyme intermediates were not significantly affected by the mutations. The double mutant Y152F+Y215F showed only a low residual activity for (*R*)-styrene oxide, with a k_{cat}/K_m value that was 6 orders of magnitude lower than with wild-type enzyme and 3 orders of magnitude lower than with the single tyrosine mutants. This indicates that the effects of the mutations were cumulative. The side chain of Gln134 is positioned in the active site of the X-ray structure of epoxide hydrolase. Mutation of Gln134 to Ala resulted in an active enzyme with slightly altered steady-state kinetic parameters compared to wild-type enzyme, indicating that Gln134 is not essential for catalysis and that the side chain of Gln134 mimics bound substrate. Based upon this observation, the inhibitory potential of various unsubstituted amides was tested, resulting in the identification of phenylacetamide as a competitive inhibitor with an inhibition constant of 30 μM.

Epoxide hydrolases catalyze the hydrolysis of epoxides to form diols without the use of a cofactor. These enzymes have been found in many organisms, including mammals, plants, insects, fungi, and bacteria (*1*−*4*). Most epoxide hydrolases play an important role in the detoxification of xenobiotic compounds, which are often degraded via reactive epoxides (*5*). Increasing attention is given to the potential use of epoxide hydrolases in the biocatalytic production of enantiopure epoxides from racemates (*6*, *7*).

We have investigated the mechanism and kinetics of the epoxide hydrolase from *Agrobacterium radiobacter* AD1, a bacterium that is able to use epichlorohydrin as its sole source of carbon and energy. The 34 kDa enzyme is enantioselective toward styrene oxide and substituted derivatives thereof (*8*). The X-ray structure was recently solved, and it shows that this epoxide hydrolase has an α/β-hydrolase fold structure (*9*, *10*), as was expected from the sequence (*2*). The three-dimensional structure consists of two domains: a main domain with a central β-sheet composed of eight strands surrounded by six α-helices and a cap domain that is composed of five α-helices, which lies on top of the main domain. The catalytic triad residues Asp107, His275, and Asp246, that were also identified by mutagenesis studies (*2*), are positioned on small loops excursing from the β-sheet. The active site is localized between the main domain and the cap domain (Figure 1).

The kinetic mechanism of epoxide hydrolase was solved in detail for both enantiomers of styrene oxide (*11*). A covalently bound ester intermediate is rapidly formed by attack of the nucleophilic Asp107 on the primary carbon atom of the epoxide ring. The Asp246−His275 pair then activates a water molecule that hydrolyzes the ester intermediate, and product is released. Hydrolysis of the covalent intermediate was the rate-limiting step for both enantiomers, causing the covalent intermediate, the alkyl-enzyme, to accumulate extensively during steady-state substrate conversion. A similar kinetic mechanism was described for the conversion of (*R*)- and (*S*)-glycidyl-4-nitrobenzoate by rat microsomal epoxide hydrolase (*12*). Since the alkylation rate of epoxide hydrolase is so high, it is expected that additional residues assist in the opening of the epoxide ring, and particularly in the protonation of the emerging oxyanion on the substrate in order to stabilize the transition state during formation of the alkyl-enzyme intermediate (*13*).

* To whom correspondence should be addressed. Phone: 31-50-3634008. Fax: 31-50-3634165. E-mail: d.b.janssen@chem.rug.nl.

10.1021/bi9922392 CCC: $19.00
Published on Web 04/13/2000

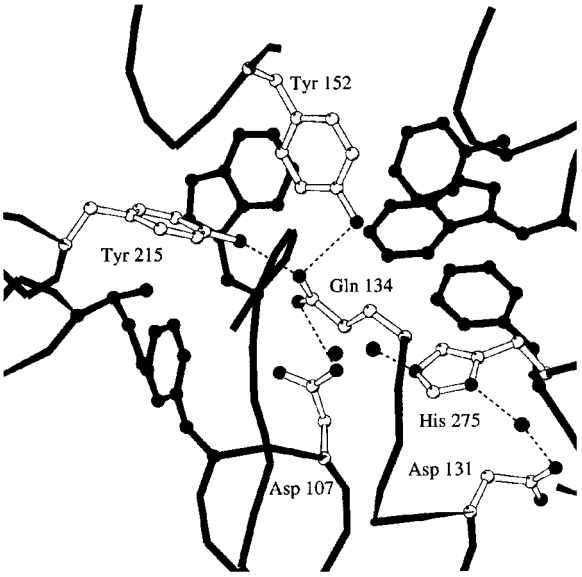

FIGURE 1: View of the active site residues as observed in the X-ray structure of epoxide hydrolase from *Agrobacterium radiobacter* AD1 (*9*). The catalytic triad residues Asp107 and His275, the position of Gln134, and the two catalytically active tyrosine residues are shown as open sticks, and the other residues are shown in black.

According to the X-ray structure of epoxide hydrolase, two tyrosine residues are probably involved in the cleavage of the epoxide ring (*9*). The phenolic hydroxyl groups of the cap domain residues Tyr215 and Tyr152 are in a position to form hydrogen bonds with the oxirane oxygen of enzyme-bound substrate. The X-ray structure suggests that the hydroxyl groups of the tyrosines can stabilize the emerging negative charge on the oxygen during formation of the alkyl-enzyme intermediate and therefore the tyrosines are probably also involved in the protonation of this intermediate to yield a stable alkyl-enzyme. Steady-state kinetic analysis of the mutants Y215F and Y152F with styrene oxide showed a major effect on the alkylation half-reaction of the mutant enzymes, indicating a role of Tyr215 and Tyr152 in protonation (*14*). To obtain a better understanding of the role of both tyrosines in the reaction mechanism of epoxide hydrolase, more insight is needed on the separate reaction steps of the catalytic cycle and the way in which they are influenced by these residues.

To study the role of Tyr215 and Tyr152 in the catalytic mechanism of epoxide hydrolase, mutant enzymes were constructed and steady-state analysis was performed in combination with pre-steady-state kinetic experiments. The role of Gln134, which also points into the active site of the X-ray structure, is investigated by site-directed mutagenesis. The position of the side chain of Gln134 could be explained by the affinity of the amide moiety for the active site tyrosine residues as indicated by inhibition studies with various unsubstituted amide molecules.

MATERIALS AND METHODS

Materials. Restriction enzymes and T4 DNA ligase were purchased from Boehringer Mannheim. The substrates (*R*)- and (*S*)-styrene oxide and the inhibitors were purchased from Aldrich. Phenylacetamide was purchased from Syncom BV (Groningen, The Netherlands). Both enantiomers of *p*-nitrostyrene oxide (97% enantiomerically pure) were synthesized as described by Westkaemper and Hanzlik (*15*). Primers for site-directed mutagenesis were obtained from Eurosequence (Groningen, The Netherlands).

Isolation of Epoxide Hydrolase and Construction of Mutants. Large quantities of pure epoxide hydrolase were obtained via a two-step purification procedure as described before (*2*). Wild-type and mutant enzyme were expressed in soluble form at a level of up to 50% of the total cellular protein content in *Escherichia coli* BL21(DE3). Enzyme was kept at 4 °C in TEMAG buffer [50 mM Tris−SO_4, pH 7.5, 1 mM EDTA, 1 mM β-mercaptoethanol, 0.02% sodium azide, and 10% (v/v) glycerol].

Mutations were made in the epoxide hydrolase gene *echA* by using uracil-containing single-stranded plasmid pEH20 (*2*) following the procedure described by Kunkel (*16*). Tyr152 was mutated to Phe with primer 5′-GAGTCGTG-GTTCTCGCAATTCC-3′ (mutated codon underlined; *14*). Tyr215 was mutated to Phe with primer 5′-CAAC-TACTTCCGTGCCAAC-3′ (*14*) and to Ala with primer 5′-CAACTACGCCCGTGCCAAC-3′ (mutated codons underlined). Gln134 was mutated to Ala with primer 5′-GATCCTATCGCCCCCGACTTT-3′ (mutated codon underlined). The Y152F+Y215F double mutant was constructed by using the unique *Xho*I restriction site that is located between the codons for Tyr152 and Tyr215 in the *echA* gene. The plasmids pEH20(Y152F) and pEH20(Y215F) were cut with *Xho*I and *Pst*I, of which the latter cuts in the ampicillin resistance gene of pEH20. The two fragments of the restricted plasmid were separated on an 0.8% agarose gel. The 1849 bp fragment of pEH20(Y152F) and the 2127 bp fragment of pEH20(Y215F) were isolated and purified by using the gel extraction kit from Promega. Subsequently, both fragments were ligated and transformed by electroporation to *E. coli* JM101. The recombinant strains contained the double mutation in the plasmid pEH20(Y152F+Y215F). Finally, all mutations were checked by sequencing of the whole gene.

Steady-State Kinetic Parameters. The steady-state kinetic parameters for the enantiomers of *p*-nitrostyrene oxide (PNSO) were determined spectrophotometrically. Substrate depletion curves were recorded in TE buffer (Tris−SO_4, pH 9.0, and 1 mM EDTA) at 30 °C on a Kontron Uvikon 930 UV/VIS spectrophotometer with a temperature-controlled cell holder by following the absorption at 310 nm. To 980 μL of TE buffer was added 10 μL of a stock solution of PNSO in acetonitrile to a final concentration of 1% (v/v) acetonitrile. The reaction was started by adding 10 μL of enzyme. The Michaelis−Menten equation was numerically fitted to the recorded traces to obtain k_{cat} and K_m values. The extinction coefficients for PNSO, $\epsilon_{310} = 4289\ M^{-1}\ cm^{-1}$, and the corresponding diol, $\epsilon_{310} = 3304\ M^{-1}\ cm^{-1}$, were used to calculate the substrate and product concentrations (*15*). The program MicroMath Scientist version 2.0 was used for all fitting purposes.

When the K_m value reached or exceeded the maximum solubility of PNSO of 1 mM, substrate depletion curves were recorded under first-order conditions with 50 μM PNSO. To obtain the k_{cat}/K_m value, the absorption (*Abs*) in time (*t*) was fitted to the single-exponential equation: $Abs = A(e^{-k[E]t}) + C$, in which *A* is the total decrease in absorption, *k* is k_{cat}/K_m, [E] is the enzyme concentration, *t* is time, and *C* is the absorption of the diol after complete conversion.

Two methods were used for the determination of the steady-state kinetic parameters of the mutant enzymes for styrene oxide (SO). In one method, the depletion of substrate was followed in time by taking samples and analyzing remaining substrate concentrations by gas chromatography (GC). Alternatively, steady-state kinetic parameters for SO were obtained from a substrate competition experiment of SO with the colorimetric substrate PNSO.

For the substrate depletion assay, 40 mL of TE buffer with an appropriate amount of one of the enantiomers of SO was incubated at 30 °C in a closed flask. A sufficient amount of enzyme was added to complete the reaction within a time course of 20 min, during which 1 mL samples were taken and added to 2 mL of ice-cold diethyl ether with 1-bromohexane as the internal standard. The samples were extracted, and the organic phase was analyzed for SO by GC using a 0.2 mm × 25 m HP-5 column and a flame-ionization detector. The integrated Michaelis−Menten equation was numerically fitted to the substrate depletion curve to yield the kinetic parameters.

Substrate competition experiments between SO and the colorimetric substrate PNSO were also carried out to obtain kinetic data for SO. When the K_m value of the enzyme for (*R*)-PNSO was below 100 μM, the colorimetric assay for PNSO was performed with 50 μM (*R*)-PNSO in the presence of 1−10 mM (*R*)- or (*S*)-SO. The recorded substrate depletion curve of (*R*)-PNSO was fitted with simple Michaelis−Menten kinetics for competing substrates (eq 1):

$$\frac{d[PNSO]}{dt} = -\frac{k_{cat}^{PNSO}[E][PNSO]}{[PNSO] + \left(1 + \frac{[SO]}{K_m^{SO}}\right)K_m^{PNSO}} \quad (1)$$

$$\frac{d[SO]}{dt} = -\frac{k_{cat}^{SO}[E][SO]}{[SO] + \left(1 + \frac{[PNSO]}{K_m^{PNSO}}\right)K_m^{SO}}$$

This approach yielded the steady-state parameters for both enantiomers of SO. With the tyrosine mutant enzymes, only the k_{cat}/K_m ratio could be determined for (*R*)-PNSO since the K_m value was higher than the solubility. Therefore, eq 1 was simplified to eq 2 to determine the kinetic parameters of SO for the various mutant enzymes:

$$\frac{d[PNSO]}{dt} = -\frac{\frac{k_{cat}^{PNSO}}{K_m^{PNSO}}[E][PNSO]}{1 + \frac{[SO]}{K_m^{SO}}} \quad (2)$$

$$\frac{d[SO]}{dt} = -\frac{k_{cat}^{SO}[E][SO]}{[SO] + K_m^{SO}}$$

This approximation is valid when (*R*)-PNSO is converted under first-order conditions ($[S] \ll K_m$) and therefore does not influence the conversion of high concentrations of SO. The colorimetric assays were performed with 50 μM (*R*)-PNSO, 5−10 mM SO, and an appropiate amount of enzyme. Equation 2 was fitted to the recorded traces to extract the k_{cat} and K_m values for the enantiomers of SO.

Product inhibition was not observed for the products of styrene oxide and *p*-nitrostyrene oxide under the assay conditions used. For wild-type enzyme, phenylethanediol when present below 50 mM did not show significant inhibition of *p*-nitrostyrene oxide (100 μM) conversion, and the product of *p*-nitrostyrene oxide did not show significant inhibition at concentrations below 10 mM. The mutant enzymes showed a similar behavior. The used substrate concentrations are lower than the tested product concentrations, and product inhibition was therefore not further considered.

Kinetic resolution of racemic epoxides by wild-type epoxide hydrolase and the Y215F mutant was performed as described before (*8*). In the case of *p*- and *m*-chlorostyrene oxide, DMSO was used as a cosolvent (10%) in order to reach a substrate concentration of 5 mM. The *E* values for *p*-nitrostyrene oxide were calculated from the k_{cat}/K_m values of the pure enantiomers in 1% acetonitrile.

Inhibition of Epoxide Hydrolase. The binding constants of unsubstituted amides to wild-type epoxide hydrolase and the Q134A mutant were determined colorimetrically by measuring the effect of different inhibitor concentrations on the conversion of (*R*)-PNSO. Depletion curves of 200 μM (*R*)-PNSO were recorded as described above with varying inhibitor concentrations. The Michaelis−Menten equation was numerically fitted to the recorded traces to obtain the k_{cat} and the apparent K_m value, K_m^{app}, at several inhibitor concentrations. The competitive inhibition constant K_i of a certain amide was obtained by fitting the formula $K_m^{app} = (1 + [I]/K_i)K_m$ to the K_m^{app} values at different inhibitor concentrations [I]. The K_m values of the Tyr215 and the Tyr152 mutants for (*R*)-PNSO could not be determined, and therefore inhibition experiments were performed under first-order conditions. Depletion curves were recorded with 50 μM (*R*)-PNSO and varying inhibitor concentrations. The apparent k_{cat}/K_m values, $(k_{cat}/K_m)^{app}$, were determined by fitting a single exponential to the recorded trace as described above. The inhibition constant K_i was obtained by fitting the formula $(k_{cat}/K_m)^{app} = (k_{cat}/K_m)/(1 + [I]/K_i)$ to the $(k_{cat}/K_m)^{app}$ values obtained at several inhibitor concentrations [I].

pH Dependence and Enzyme Inactivation. The steady-state kinetic parameters of wild-type and mutant enzyme for (*R*)-PNSO in the pH range 5−11 were determined with the colorimetric assay described under "Steady-State Kinetic Parameters". The following buffers were used: pH 5−6, 50 mM potassium acetate; pH 6−7.5, 50 mM potassium phosphate; pH 7.5−9, 50 mM Tris−SO_4; pH 9−11, 50 mM glycine−NaOH. Each buffer contained 1 mM EDTA. The k_{cat}/K_m data (*k*) were fitted with eq 3 in which k_{max} is the maximum value that can be reached by k_{cat}/K_m, K_{a1} and K_{a2} are the ionization constants, and *x* is an additional parameter which is used to fit the steep decrease of k_{cat}/K_m at high and increasing pH values. The ionization parameter K_{a2} has no physical meaning in the context of the formula and is just used to fit the data at high pH values. Fitting of the k_{cat}/K_m data with the adjusted double ionization formula gives a reliable value for K_{a1}.

$$k = \frac{k_{max}}{1 + \frac{[H^+]}{K_{a1}} + \left(\frac{K_{a2}}{[H^+]}\right)^x} \quad (3)$$

Irreversible inactivation of enzyme at a certain pH was determined by incubating concentrated enzyme at 30 °C. Samples were taken at different times and diluted in TE buffer of pH 9.0. The remaining activity k of each sample was determined with (*R*)-PNSO at pH 9. The enzyme inactivation rate (k_{inact}) at a particular pH value was obtained by fitting the k data against time (t) with the single exponential $k = k_{cat}(e^{-k_{inact}t})$. The enzyme inactivation rates were used in the fitting of the substrate depletion curves of (*R*)-PNSO to obtain k_{cat}/K_m data that were corrected for irreversible enzyme inactivation.

Circular Dichroism. Far-UV circular dichroism spectra were recorded on a AVIV 62A DS spectrometer by measuring the ellipticity in millidegrees. Enzyme was dialyzed against 5 mM phosphate buffer, pH 7.0, and spectra were recorded in a 1 mm cuvette at 25 °C. The CD spectra were corrected for buffer absorption. Temperature curves were recorded at 222 nm between 10 and 80 °C with steps of 1 °C, and the signal was averaged at each step for 30 s.

Stopped-Flow Fluorescence. Stopped-flow fluorescence experiments were performed at 30 °C on an Applied Photophysics model SX.17MV apparatus. The tryptophan residues were excited at a wavelength of 290 nm, and the resulting fluorescence emission was recorded after passage through a 305 nm cutoff filter. Stock solutions of (*R*)- and (*S*)-SO and (*R*)-PNSO were prepared in acetonitrile and were freshly diluted in TE buffer to a final concentration of 1% (v/v) acetonitrile. All mentioned concentrations are those after mixing.

Multiple-turnover experiments were done with 10 μM enzyme and 0.5−10 mM (*R*)- or (*S*)-SO. The recorded fluorescence signal (F) in time (t) was fitted with a double exponential of the form $F = A1(e^{-k_{obs1}t}) + A2(e^{-k_{obs2}t}) + C$, in which $A1$ and $A2$ are amplitudes, k_{obs1} and k_{obs2} are the observed rate constants, and C is the floating end point (*11*). The amplitudes $A1$ and $A2$, which are dependent on the substrate concentration [S], were described by a hyperbola of the form $A = b[S]/(d + [S])$, in which b and d are constants. The two observed rate constants k_{obs1} and k_{obs2} are described as an analytical function of the kinetic constants as shown in eq 4 (*11*, *17*, *18*):

$$k_{obs1,2} = 0.5P \pm 0.5\sqrt{P^2 - 4Q}$$

$$P = k_2\frac{[R]}{K_s + [R]} + k_{-2} + k_3 + k_{-3} + k_4 \qquad (4)$$

$$Q = k_2(k_3 + k_{-3} + k_4)\frac{[R]}{K_s + [R]} + k_{-2}(k_{-3} + k_4) + k_3k_4$$

By combining these equations, the multiple-turnover fluorescence traces recorded at different substrate concentrations were directly described as a function of kinetic constants. The fitting was restricted by using the experimentally determined steady-state k_{cat} and K_m, which are functions of the rate and equilibrium constants according to eqs 5 and 6 (*11*):

$$k_{cat} = \frac{k_2k_3k_4}{k_{-2}(k_{-3} + k_4) + k_2(k_3 + k_{-3} + k_4) + k_3k_4} \qquad (5)$$

$$K_m = \frac{K_s(k_{-2}k_{-3} + k_{-2}k_4 + k_3k_4)}{k_{-2}(k_{-3} + k_4) + k_2(k_3 + k_{-3} + k_4) + k_3k_4} \qquad (6)$$

As a final restriction, we used the requirement that the obtained set of rate constants must describe the experimental fluorescence traces by using the reaction mechanism of Scheme 1, in which [ER] is the Michaelis complex and E−R1 and E−R2 are two kinetically distinct states of the covalent intermediate. The multiple-turnover reactions were simulated with a set of kinetic constants, and the appropiate enzyme and substrate concentrations and the concentrations of all enzyme species at each time point were calculated. For each time point, the concentration of each enzyme species was divided by the total enzyme concentration and multiplied by a fluorescence factor that is specific for each enzyme species, yielding a relative fluorescence trace. The latter was multiplied by the fluorescence signal of enzyme without substrate to fit it to the experimental trace. A unique set of fluorescence factors that could be used to fit all multiple-turnover traces were calculated from the fit of the data.

RESULTS

Role of Tyrosines in Epoxide Hydrolases. The X-ray structure of epoxide hydrolase from *A. radiobacter* AD1 was recently determined (*9*). This enabled the identification of additional residues besides the catalytic triad that may have a function in enzyme catalysis (*9*). The active site is lined mainly with hydrophobic residues, except for the catalytic triad residues and two tyrosines (Figure 1). The two tyrosine residues, Tyr152 and Tyr215, are located in the first and the fifth α-helix of the cap domain, which is composed of a total of five helices. These tyrosines are the only acidic groups present in the active site that could be responsible for protonation of the substrate during the formation of the alkyl-enzyme intermediate. A role of these tyrosines in protonation or hydrogen bond donation was also suggested by the presence of Gln134 in the proposed active site. The side chain of Gln134 occupies the space where substrate is expected to bind and the amide oxygen is hydrogen bonded to Tyr152 and Tyr215. The presence of Gln134 in the active site was accompanied by a structural distortion possibly caused by crystal contacts (*9*). Thus, the three-dimensional structure of epoxide hydrolase suggests an important role in catalysis for Tyr152 and Tyr215, and no clear function for Gln134.

If Tyr152 and Tyr215 are important residues in the reaction mechanism of epoxide hydrolase, it can be expected that they are conserved in other epoxide hydrolases. Epoxide hydrolases have been divided into two classes based on homology and properties, namely, the soluble and the microsomal epoxide hydrolases. Sequence similarities between the epoxide hydrolases are often only 20−30%, and they are particulary poor in the cap domain region. Tyr215 is located in the C-terminal part of the cap domain, and a sequence alignment shows that it is absolutely conserved in eukaryotic and microbial epoxide hydrolases, which supports an important role for Tyr215 (Figure 2). A short stretch of sequence that is different for soluble and microsomal epoxide hydrolases, namely, N-W/Y-Y-R and R-F/Y/L-Y-K/A, respectively, allows the identification of the conserved Tyr (underlined) in other epoxide hydrolases.

Scheme 1

$$E + R \overset{K_S}{\rightleftharpoons} [ER] \underset{k_{-2}}{\overset{k_2}{\rightleftharpoons}} E\text{-}R1 \underset{k_{-3}}{\overset{k_3}{\rightleftharpoons}} E\text{-}R2 \xrightarrow{k_4} E + P$$

Tyr152 is located in the N-terminal part of the cap domain, and the sequence alignment shows that it is conserved among the soluble epoxide hydrolases from mammals and plants (Figure 2). It is not clearly present in the epoxide hydrolase from *Corynebacterium*, which appears to have a histidine residue at this position. There are indications from the alignment results that an equivalent of Tyr152 is also present in microsomal epoxide hydrolases from mammals and insects. Two tyrosines are conserved in the N-terminal part of the cap domains of the microsomal epoxide hydrolases, of which Tyr299 may be located in the active site (Figure 2). Alignments between the soluble and the microsomal epoxide hydrolases are particularly poor in this part of the sequence. The N-terminal part of the cap domain of the microsomal epoxide hydrolases appears to be larger in sequence than that of the soluble epoxide hydrolases and might have a different topology. Thus, Tyr215 is present in all epoxide hydrolases, and Tyr152 is at least partly conserved, indicating that a selective pressure preserved these residues during evolution of these enzymes.

Residue Gln134, which is pointing into the active site in the crystal structure, is not conserved in the other epoxide hydrolase sequences (Figure 2). The alignment shows that an Asp or Asn residue is present at the same position in the soluble epoxide hydrolases except for the *Corynebacterium* enzyme. The conservation of Pro135 in the soluble epoxide hydrolases indicates that the side chains of Gln, Asp, or Asn, which are positioned next to this conserved Pro, may serve some structural role. No conserved Gln residue is found in the N-terminal part of the cap domains of the microsomal epoxide hydrolases.

Mutation of Active Site Tyrosines. To investigate the function of Tyr152 and Tyr215 in the reaction mechanism of epoxide hydrolase, mutant enzymes were constructed. Tyr215 was mutated to Phe (*14*) and Ala, Tyr152 was mutated to Phe (*14*), and the double mutant Y152F+Y215F was constructed. The mutant enzymes were all well expressed in *E. coli* BL21(DE3) in soluble form and in quantities of up to 50% of the total cellular protein. Circular dichroism (CD) spectroscopy was used in order to assess the structural integrity of the purified tyrosine mutant enzymes. Spectra were recorded in the far-UV region between 190 and 250 nm (Figure 3). The spectra of wild-type enzyme, Y215F, Y152F, and the double mutant Y152F+Y215F overlap perfectly, indicating that the mutant enzymes and the wild type have identical overall structures.

The structural integrity of the tyrosine mutants was further examined by determining their thermostability. Temperature melting curves were recorded between 10 and 80 °C for the wild-type enzyme, the Y215F mutant, and the double mutant by following the ellipticity changes at 222 nm on the CD spectrometer. Wild-type and mutant enzymes showed identical curves until the enzymes precipitated at temperatures between 62 and 67 °C. The curves were not sigmodal, and therefore an accurate determination of the melting temperature was not possible. However, the point of precipitation was reproducible in each case and was even several degrees higher for the mutant enzymes than for wild type. Thus, the Y215F and Y152F+Y215F mutants appear to be more thermostable than the wild-type enzyme.

Activities of Tyrosine Mutants. The steady-state kinetic parameters of the Tyr152 and Tyr215 mutants were determined for the enantiomers of styrene oxide (SO) and *p*-nitrostyrene oxide (PNSO). The Y215F, Y215A, and Y152F mutations resulted in enzymes with dramatically changed steady-state kinetics, but they were still catalytically active (Table 1). As shown previously, the k_{cat}/K_m values for the tested substrates were 3 orders of magnitude lower for these mutant enzymes than for wild-type enzyme (*14*). This large change originated mainly from the increase of the K_m values of the mutant enzymes since the k_{cat} values for the (*R*)-enantiomers of SO and PNSO were only 2- and 4-fold lower, respectively, for the Tyr mutants than for wild type. The k_{cat} values for the (*S*)-enantiomers were much more affected by the mutation. The mutation of Tyr215 to either Phe or Ala resulted in mutants with similar steady-state parameters, indicating that the removal of a phenyl ring from the active site of the Y215F mutant did not further affect catalysis. The Y152F mutant was a poorer catalyst than the Y215F and Y215A mutants, as was clear from the 2-fold lower k_{cat} and 6-fold higher K_m for (*R*)-SO.

The k_{cat}/K_m values of the Y215F and Y152F mutants for the (*S*)-enantiomers had decreased more than the k_{cat}/K_m values for the (*R*)-enantiomers, and as a result the enantioselectivities for racemates were increased as was apparent from the larger *E* values (*14*). The *E* values of the Y215F mutant were increased 2−4-fold for the tested substrates (Table 2). The Y215A mutant had a lower enantioselectivity for SO and PNSO than wild-type enzyme. These low *E* values originated from the relatively high k_{cat}/K_m values of the Y215A mutant for the (*S*)-enantiomers compared to the Y215F mutant, whereas the k_{cat}/K_m values of these mutants for the (*R*)-enantiomers were similar. Likely, the Y215A mutant has an enlarged active site cavity which accommodates the (*S*)-enantiomers better.

High concentrations of the Y152F+Y215F mutant were needed to detect enzyme activity and to compete with the slow spontaneous hydrolysis of the substrate. The kinetics of the double mutant clearly showed that the effect of mutations was cumulative (Table 1). The k_{cat}/K_m values for the single mutants decreased 3 orders of magnitude compared to wild-type enzyme, while it decreased 6 orders of magnitude for the double mutant. These data indicate that Tyr215 and Tyr152 have an important and additive function in the reaction mechanism of epoxide hydrolase, and that the presence of a single Tyr residue results in an enzyme that can still catalyze the hydrolysis of epoxides effectively, although with decreased substrate affinity.

pH Dependence. The pH dependence of the k_{cat}/K_m values of wild-type enzyme and the Y152F and Y215F mutants for (*R*)-PNSO was studied to obtain more information about the residues involved in catalysis. Despite the 1000-fold difference between the k_{cat}/K_m values of wild-type and mutant enzymes, the three enzymes behaved similarly with changing pH and they had a broad optimum between pH 6 and 10 (Figure 4). The k_{cat}/K_m decreased rapidly on both sides of the pH optimum, indicating that the changed ionization state of certain residues resulted in the inactivation of enzyme.

```
                «««««««««««««««««««««« cap domain »»»»»»»»»»»»»»»»»»»»
Agr-sEH  134 QPDFGPV--YFGLGHVHESWY-SQFHQ---LDMA <45> NIHGGFNYYRANIRPDAALWTDLDHTMSDLPVT 239
Cor-sEH  126 PGLIKAG-DSFPIPVALMINH-IFFHGG---NPD <46> SIRSGCQWYATGLREDTENLAKATD-KLTIPVI 232
Ara-sEH  136 DPSVKPVDRMRA--FYGDDYYICRFQEFGDVEAE <59> GFSGPVNYYR-NFNRNNELLGPWVGSKIQVPTK 258
Soy-sEH  157 DPNIRTVDGMRA--LYGDDYYVCRFQKPGEMEAQ <58> GFTGPLNYYR-NFNLNWELTAPWTGGQIKVPVK 278
Pot-sEH  136 NPKMNVVEGLKA--IYGEDHYISRFQVPGEIEAE <59> GFTGAVNYYR-ALPINWELTAPWTGAQVKVPTK 258
Tob-sEH  132 GPETFP----RD--LIPNGFYMLRWQEPGRAEKD <61> FRTALQVPYR-AWLEEYGV----KDIKVKVPCL 248
Hum-sEH  365 NPNMSPLESIKANPVFDYQLY---FQEPGVAEAE <61> GFRGPLNWYR-NMERNWKWACKSLGRKILIPAL 488
Mou-sEH  363 DPDVSPMKVIRSIPVFNYQLY---FQEPGVAEAE <62> GFRGPLNWYR-NTERNWKWSCKGLGRKILVPAL 487
Rat-sEH  364 NPEVSPMEVIRSIPVFNYQLY---FQEPGVAEAE <62> GFRGPLNWYR-NTERNWKWSCKALGRKILVPAL 488

Hum-mEH  279 VELLYPVKEKVFYSLMRESGYMHIQCTKPDTVGS <53> TIISSQRFYKEN-LGQGWMTQKHERMKVYVPTG 397
Rab-mEH  279 MELLYPFKEKVFYSLMRESGYMHIRATKPDTVGC <53> SIVSSQRYYKEN-LGQGFMAHKHERLKVHVPTG 397
Rat-mEH  279 IELLYPYKEKVFYSIMRESGYLHIQATKPDTVGC <53> TIVSSQRYYKEN-LGQGIMVHKHEGMKVFVPTG 397
Mou-mEH  279 IELLYPYKEKVFYSIMRESGYLHIQATKPDTVGC <53> TIVSSQRFYKEN-LGQGVMVHRHEGMKVFVPTG 397
Pig-mEH  279 LELLYPFK-KTFYTLMRESGYMHIQSTKPDTVGC <53> TITSSQRFYKEN-LGQGVMANKHEAIKVHVPTG 396
Hor-mEH  279 MDRIYPLKNL-FSYILRETGYFHIQATKPDTIGV <52> CIVTSTRLYAEG-FSWPEVLIVHR-IPSMVPTA 394
Cab-mEH  280 -ERLYPLSTR-FANLLRETGYMHIQSTKPDTVGV <53> AITPAMRLYAEN-FNKRTVEMKLDEIPTPVPTW 396
                yp            Y                       Y                    vP
```

FIGURE 2: Sequence alignment of the microsomal and soluble-like epoxide hydrolases. The sequences were aligned using the multiple alignment program ClustalW. The N-terminal regions of the aligned microsomal epoxide hydrolases were aligned with the N-terminal regions of the soluble epoxide hydrolases by hand. The N-terminal and C-terminal sequences of the cap domain are shown, according to the X-ray structure of the epoxide hydrolase from *Agrobacterium radiobacter* AD1 (*9*). The residues that belong to the cap domain region are indicated in broken brackets. The epoxide hydrolase sequences are divided into two classes, namely, the soluble and the microsomal epoxide hydrolases based on homology and properties. The soluble epoxide hydrolases (sEH) are from *Agrobacterium radiobacter* AD1 (2292731), *Corynebacterium* sp. (2897599), *Arabidopsis thalania* (2760840), Soybean (1304227), Potato (407942), Tobacco (1354849), Human (462369), Mouse (1708375), Rat (462371). The microsomal epoxide hydrolases (mEH) are from Human (123926), Rabbit (123927), *Rat* (123928), Mouse (1890860), Pig (1840391), Hornworm (2144482), Cabbage looper (2661096). The sequence ID (GenBank) is shown in parentheses, and the letters that are used to name the organism in the figure are shown underlined. Conserved residues are shown in boldface type, and the conserved tyrosine residues are underlined.

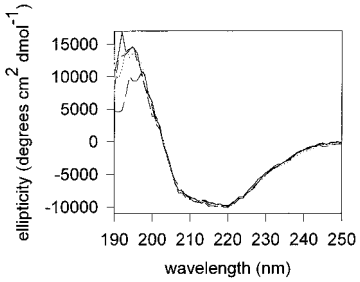

FIGURE 3: Circular dichroism spectra of wild-type enzyme (solid line), the Y215F mutant (dashed line), the Y152F mutant (dashed line), and the Y152F+Y215F double mutant (dotted line). Spectra were recorded with 10 μM enzyme between 190 and 250 nm at 25 °C in 5 mM phosphate buffer, pH 7.0.

At low pH, the k_{cat}/K_m ratio decreased in a way that corresponded to a single-ionization event, as is evident from a slope of 1 in the log(k_{cat}/K_m) versus pH plot (Figure 4). A pK_a value of 5.8 was fitted for wild-type enzyme and the Y215F mutant. This pK_a is typical for a His residue and may reflect the pK_a of the catalytic His275, since this residue would not be capable of activating a water molecule for the hydrolysis of the covalent intermediate when it is protonated at low pH.

Above pH 10, the k_{cat}/K_m drops very fast with increasing pH both for the wild-type enzyme and for the single tyrosine mutants. The k_{cat}/K_m data of the Y152F mutant could not be determined accurately at pH values above 10 due to the interference of the high amounts of enzyme needed for the spectroscopic assay at these pH values, but the Y152F mutant showed a similar broad pH optimum as for the wild-type and Y215F mutant enzymes. The slope of decline in the log(k_{cat}/K_m) versus pH plot was found to be close to 4 for the wild-type enzyme and the Y215F mutant when eq 3 was used to fit the data (Figure 4). The fast decline cannot be explained by a simple single or double ionization process. Since the form of the curve is similar for wild-type enzyme and the mutants, other residues than Tyr152 or Tyr215 also seem to be involved in the reversible decrease of activity at high pH. Therefore, this part of the pH curve did not yield clear information about residues involved in catalysis. However, the pK_a value of the proton-donating group had to be higher than 10, leaving the active-site-located tyrosines as the best candidates, since the pK_a value of tyrosine is usually in the range of 9−11.

Besides reversible reduction of enzyme activity above pH 10, irreversible inactivation also took place at high pH. The irreversible inactivation rates of the wild-type and mutant enzymes were determined by measuring the change in the k_{cat}/K_m values at pH 9.0 for enzyme that was first preincubated at a certain pH for different time periods (Figure 5). The K_m of the wild-type enzyme for (*R*)-PNSO did not change after incubation at high pH, indicating that the lowered k_{cat}/K_m values were a result of a lowered k_{cat} due to enzyme inactivation. The rate of irreversible inactivation for wild-type enzyme increased rapidly above pH 10, but the inactivation rates for the Y215F and the Y152F mutant remained low at increasing pH. This means that the Tyr mutants are more stable than wild-type enzyme at higher pH.

The irreversible inactivation rates suggest that the presence of two tyrosines in the active site causes the observed inactivation of wild-type enzyme, since the single tyrosine mutants show only little inactivation. Likely, the presence of two deprotonated tyrosine residues in the active site of wild-type enzyme at high pH causes the enzyme to unfold, whereas one deprotonated tyrosine in the single tyrosine mutants only leads to minor inactivation. The pK_a values of Tyr152 and Tyr215 in wild-type enzyme can be estimated by linking the irreversible inactivation rates to the ionization state of the two tyrosines (eq 7). The formula for a standard two-step ionization process was simplified by assuming that

Table 1: Steady-State Parameters of Wild-Type and Mutant Epoxide Hydrolase for the Enantiomers of Styrene Oxide and *p*-Nitrostyrene Oxide

	(*R*)-styrene oxide			(*S*)-styrene oxide			(*R*)-*p*-nitrostyrene oxide			(*S*)-*p*-nitrostyrene oxide		
	k_{cat} (s^{-1})	K_m (mM)	k_{cat}/K_m (mM^{-1} s^{-1})	k_{cat} (s^{-1})	K_m (mM)	k_{cat}/K_m (mM^{-1} s^{-1})	k_{cat} (s^{-1})	K_m (mM)	k_{cat}/K_m (mM^{-1} s^{-1})	k_{cat} (s^{-1})	K_m (mM)	k_{cat}/K_m (mM^{-1} s^{-1})
wild type[c]	3.8	0.0005	8000	10.5	0.021	500	7.8	0.008	975	>7.7	>0.5	13.1[a]
Y215F[c]	2.5	0.6	4.2	0.7	5	0.14	>3.4	>0.8	4.2[a]	>0.02	>1	0.02[a]
Y215A	1.7	0.6	3	0.6	2.4	0.25	>1.6	>0.8	2[a]	>0.17	>1	0.17[a]
Y152F[c]	1.1	3.5	0.3	>0.12	>15	0.008[a]	>1.2	>1.5	0.8[a]	>0.005	>1	0.005[a]
Y152F+Y215F	>0.015	>30	0.0005[a]	—[b]	—	—	>0.003	>3	0.001[a]	—	—	—
Q134A	0.8	0.001	800	1.4	0.07	20	2.2	0.009	240	>1	>1	1

[a] Due to high K_m values and the maximum solubility of *p*-nitrostyrene oxide (1 mM) and styrene oxide (10 mM), only the k_{cat}/K_m values could be determined, setting lower limits for the k_{cat} and K_m values. [b] Not detectable (—). [c] Data from Rink et al. (*14*).

Table 2: Enantioselectivity of the Y215F Mutant and Wild-Type Enzyme

	E value	
	wild type	Y215F
p-nitrostyrene oxide	100	>200
styrene oxide	16	30
m-chlorostyrene oxide	6.5	12
p-chlorostyrene oxide	32	130

only the double-ionized form of the enzyme (E^{2-}) inactivates with the rate constant $k_{i,E^{2-}}$ (*19*). A single-ionization process could not describe the pH inactivation data of wild-type enzyme.

$$k_{inact} = \frac{k_{i,E^{2-}} K_1 K_2}{K_1 K_2 + K_1[H^+] + [H^+]^2} \quad (7)$$

The fitting of the inactivation constants, k_{inact}, at various pH values with eq 7 resulted in a pK_{a1} value of 10.9 and pK_{a2} values of 11.5−13.5. The value for pK_{a2} was dependent on the exact value of $k_{i,E^{2-}}$ for which only the lower limit of 0.1 s^{-1} could be estimated from experiments that were performed at higher pH values. Increasing the value for $k_{i,E^{2-}}$ only increased the pK_{a2} to a maximum of 13.5 and did not affect pK_{a1}. Thus, the pK_a value of the proton-donating tyrosine was estimated to be 10.9.

Pre-Steady-State Kinetics of the Tyrosine Mutants with Styrene Oxide. Stopped-flow fluorescence experiments under multiple-turnover conditions were performed with the Y152F, Y215F, and Y215A mutants with (*R*)-SO and (*S*)-SO to obtain information about the kinetics of the separate reaction steps and to understand how the tyrosine residues are involved in the kinetic mechanism of epoxide hydrolase. Multiple-turnover experiments were performed with 10 μM enzyme and 0.5−10 mM (*R*)-SO and (*S*)-SO (Figures 6 and 7). The pre-steady-state kinetics of wild-type enzyme for (*R*)-SO and (*S*)-SO were analyzed before using substrate concentrations of 5−50 μM. These low substrate concentrations were sufficient, since the K_m values of epoxide hydrolase for the (*R*)- and (*S*)-enantiomers were low, 0.46 and 21 μM, respectively (*11*). The K_m values for the enantiomers of SO were at least 100-fold higher with the tyrosine mutants, and therefore substrate concentrations in the millimolar range were needed to detect changes in the protein fluorescence signal upon conversion.

The Y152F mutant showed only minor changes of the protein fluorescence upon conversion of 10 mM (*R*)-SO and

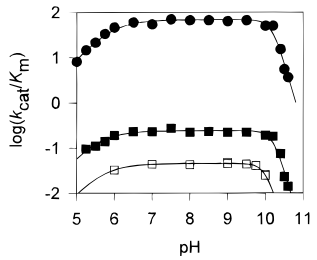

FIGURE 4: pH dependency of the steady-state parameters of the wild-type and the single tyrosine mutant enzymes. The effect of pH on log(k_{cat}/K_m) of the wild-type enzyme (●), the Y215F mutant (■), and the Y152F mutant (□) was determined with (*R*)-PNSO at 30 °C. The solid lines are fits of the data to eq 3. The solid line for the Y152F mutant was obtained by using the same parameters in eq 3 as for the wild-type and the Y215F mutant enzyme except for k_{max}.

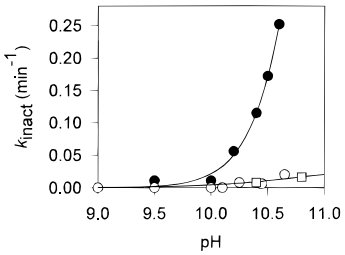

FIGURE 5: Irreversible inactivation rates of wild-type and the single tyrosine mutant enzymes at various pH values. The symbols indicate wild-type enzyme (●), the Y215F mutant (○), and the Y152F mutant (□). The solid line for wild-type enzyme shows a fit of the data with the formula of eq 7 and a pK_{a1} of 10.9 and a pK_{a2} of 11.5−13.5. The solid line that fits the data for the Y215F and Y152F mutants is a simple exponential fit to link the data points.

(*S*)-SO, resulting in almost flat fluorescence traces. The high K_m values of the Y152F mutant for both enantiomers of SO cause only a small fraction of the enzyme to interact with substrate, and therefore free enzyme predominates the fluorescence signal in the stopped-flow experiments. Another limiting factor in observing fluorescence changes was the maximum concentration of 10 mM that could be obtained for SO. Thus, it was not possible to analyze the pre-steady-state kinetics of the Y152F mutant.

The Y215F and Y215A mutants had a K_m value of 0.6 mM for (*R*)-SO, and as a result, wild-type-like fluorescence traces were recorded that could be used for further analysis (Figure 6). The K_m values of the Y215F and Y215A mutants for (*S*)-SO were higher, 5 and 2.4 mM, respectively. The Y215F mutant therefore showed only little quenching of the protein fluorescence when mixed with 10 mM (*S*)-SO. Mixing of the Y152A mutant with 10 mM (*S*)-SO resulted

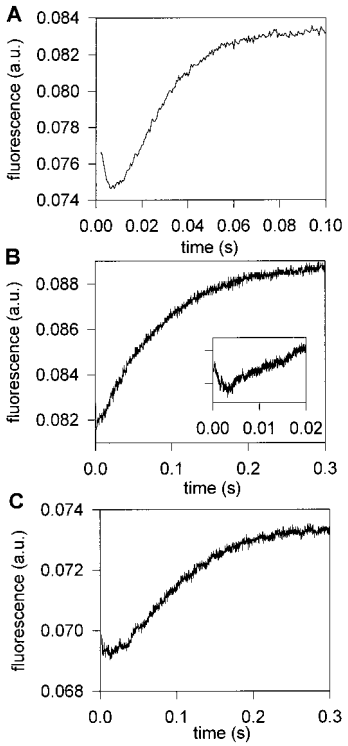

FIGURE 6: Fluorescence traces of multiple turnovers of (*R*)-SO by wild-type and mutant enzymes. The experiments were done on a stopped-flow fluorescence apparatus at 30 °C in TE buffer, and the displayed traces are representative for all the traces recorded with different substrate concentrations for that particular experiment. (A) Fluorescence trace recorded with 0.5 μM wild-type enzyme with 10 μM substrate (*11*). (B) Fluorescence trace recorded with 10 μM Y215F mutant enzyme with 5 mM substrate. The inset displays the small fluorescence dip after averaging of 8 fluorescence traces. (C) Fluorescence trace recorded with 10 μM Y215A mutant enzyme with 10 mM substrate.

in a significant decrease of the intrinsic protein fluorescence (Figure 7).

The kinetic mechanism of wild-type enzyme for the conversion of (*R*)-SO comprised four reaction steps as shown in Scheme 1 (*11*). The stopped-flow fluorescence traces that were recorded for the conversion of (*R*)-SO by the Y215F and Y215A mutants resembled those of wild-type enzyme, indicating that a four-step reaction mechanism is also needed for the mutant enzymes (Figure 6). Besides, it was not possible to fit the fluorescence data of the mutant enzymes to a three-step mechanism. The quenching of the protein fluorescence was smaller for the Y215F and Y215A mutants than for the wild-type enzyme (Figure 6). This indicates that the first covalent intermediate (E−R1), that causes the fluorescence quenching (*11*), hardly accumulates in the pre-steady-state phase.

The pre-steady-state kinetics of wild-type enzyme for (*R*)-SO were previously solved by separately fitting each multiple-turnover trace which was obtained by stopped-flow fluorescence with a double exponential. This yielded two observed rate constants for each substrate concentration (k_{obs1} and k_{obs2}) with amplitudes of opposite signs (*11*). By using the analytical solutions for k_{obs1} and k_{obs2} (eq 4) and the steady-state kinetic parameters, the kinetic constants for the conversion of (*R*)-SO by wild-type enzyme could be obtained from the observed rate constants (Table 3). A somewhat different combined approach was used to determine the

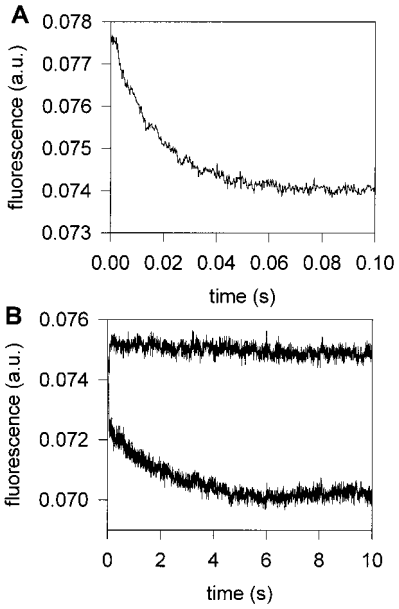

FIGURE 7: Fluorescence traces of multiple turnovers of wild-type and mutant enzyme with (*S*)-SO. The experiments were done on a stopped-flow fluorescence apparatus at 30 °C in TE buffer, and the displayed traces are representative for all the traces recorded with different substrate concentrations at that particular experiment. (A) Fluorescence trace recorded with 0.5 μM wild-type enzyme and 25 μM substrate (*11*). (B) Fluorescence traces recorded with 10 μM Y215F (upper line) and Y215A (lower line) mutant enzymes with 10 mM substrate.

kinetic constants for the conversion of (*R*)-SO by the Y215F and the Y215A mutants.

As mentioned before, the quenching of the protein fluorescence of the Y215F and Y215A mutants when mixed with (*R*)-SO was small and fast compared to the slow and large increase of the protein fluorescence that followed. Therefore, fitting of a double exponential function to the separate fluorescence traces resulted in variable k_{obs1} data, and, consequently, the k_{obs2} data were also affected. The k_{obs2} data exhibited saturation behavior for both mutant enzymes, but the scattering in the data made further processing of the data difficult. This problem was overcome by simultaneous fitting of all the fluorescence traces, which were recorded with different substrate concentrations, to a double exponential in which the observed rate constants k_{obs1} and k_{obs2} are described as a function of the kinetic constants and substrate concentration (eq 4). Solutions for the kinetic constants were further restrained by the experimentally measured steady-state k_{cat} and K_m values (Table 1) using eqs 5 and 6. By fitting all the experimental data simultaneously, the kinetic constants of the Y215F and Y215A mutants for (*R*)-SO were directly obtained from a set of fluorescence traces recorded at different substrate concentrations. Finally, the kinetic constants that were obtained from this analytical procedure were tested for their ability to simulate the multiple-turnover experiments with the reaction mechanism of Scheme 1. Fluorescence factors were used for each enzyme species to fit the simulation to the experimental fluorescence trace (*11*). The fluorescence factors for the species E−R1 and E−R2 were 0.9 and 1.3 for the Y215F mutant and 0.95 and 1.2 for the Y215A mutant. Adjustment of the fluorescence factors was necessary to obtain adequate fits, since the fluorescence factors of wild-type enzyme,

Table 3: Pre-Steady-State Rate Constants for the Conversion of (*R*)-SO and (*R*)-PNSO by Wild-Type Enzyme and the Tyr215 Mutants

(*R*)-SO[b]	K_S (μM)	k_2 (s^{-1})	k_2/K_S (μM^{-1} s^{-1})	k_{-2} (s^{-1})	k_3 (s^{-1})	k_{-3} (s^{-1})	k_4 (s^{-1})
wild type[a]	90 ± 10	1100 ± 100	12.2 ± 1	40 ± 5	70 ± 5	<4	4.2 ± 0.2
Y215F	1200 ± 300	60 ± 20	0.05 ± 0.03	150 ± 50	35 ± 5	<0.5	8 ± 1
Y215A	3500 ± 500	40 ± 15	0.01 ± 0.003	14 ± 4	12 ± 6	3 ± 0.5	3.5 ± 0.5
(*R*)-PNSO[c]							
wild type	>500	>825	1.65	2	9	–	–

[a] Data taken from Rink and Janssen (*11*). [b] The data belong to a four-step mechanism as shown in Scheme 1. [c] The data belong to a three-step mechanism as shown in Scheme 2.

which are 0.85 and 1.1 for the intermediates E−R1 and E−R2, respectively, were not applicable to the mutant enzymes (*11*). This approach resulted in a unique solution of the rate constants for the Y215F and Y215A mutants for the conversion of (*R*)-SO (Table 3).

The largest difference between the kinetic constants of wild-type enzyme and the Tyr215 mutants was found in the first part of the catalytic cycle, namely, the substrate binding and the reversible alkylation steps, also referred to as alkylation half-reaction (Table 3). The binding constants of the Y215F and Y215A mutants for (*R*)-SO are 15- and 40-fold higher, respectively, than the K_S of wild-type enzyme for (*R*)-SO, indicating that Tyr215 is involved in substrate binding. The subsequent alkylation step is also affected by the mutation of Tyr215 to Phe and Ala. The alkylation rates are down by a factor of 20, but they have not become rate-limiting. Surprisingly, the dealkylation rate (k_{-2}) of the covalent intermediate for the Y215F mutant is faster than its alkylation rate, and as a result, the covalent intermediate hardly accumulates in this mutant. This caused the small fluorescence dip that was observed for this mutant (Figure 6B). The Y215A mutant has a lower dealkylation rate compared to the alkylation rate, as is the case in wild-type enzyme, and therefore the first covalent intermediate still accumulates to a small extent.

The second part of the reaction mechanism of the Y215F and Y215A mutants for the conversion of (*R*)-SO, or the so-called hydrolytic half-reaction which comprises the unimolecular isomerization step and the hydrolysis step, is also affected by the mutation. The unimolecular isomerization step (k_3) has become slower for both mutants compared to wild-type enzyme. The Y215A mutant is most affected, but since the nature of the unimolecular isomerization is not known, it is unclear what caused this change. Hydrolysis of the alkyl-enzyme intermediate is the rate-limiting step in wild-type enzyme for the conversion of (*R*)-SO, and although the hydrolysis step has the lowest rate in the catalytic cycle of the Y215F and Y215A mutants, it is not the sole rate-limiting step. The hydrolysis rates of the covalent intermediate (k_4) are 2 and 3 times higher than the overall k_{cat} for the Y215A and Y215F mutants, respectively.

The individual rate constants could not be determined for the conversion of (*S*)-SO by the Y215A mutant although quenching could be observed (Figure 7). The conversion of the 1.5% (*R*)-SO that is present in commercial (*S*)-SO interfered too much with the fluorescence signal.

Pre-Steady-State Kinetics of Wild-Type Enzyme with (R)-PNSO. To understand how the K_m values for (*R*)-PNSO could change 3 orders of magnitude without affecting the k_{cat}, more insight is needed in the rates of the separate reaction steps. Multiple-turnover experiments were performed with 1 μM wild-type enzyme and 25−500 μM (*R*)-PNSO, and the fluorescence emission was followed in time. The conversion of substrate resulted in quenching of the protein fluorescence, and the resulting traces could be fitted with a single-exponential function to yield a k_{obs} (Figure 8). The k_{obs} data followed a linear relationship with (*R*)-PNSO concentration, indicating that enzyme was not saturated with substrate at concentrations up to 300 μM. At higher substrate concentrations, the fluorescence quenching occurred mainly in the dead time of the apparatus, and therefore no accurate values could be obtained for the k_{obs}. The minimal scheme to describe the data is a three-step reaction mechanism (Scheme 2). First, substrate is bound according to a rapid equilibrium to form a Michaelis complex ([ES]), which does not quench the fluorescence signal (*11*). Then, the alkyl-enzyme intermediate (E−S) is formed in a reversible reaction step, and finally the intermediate is hydrolyzed to yield product and free enzyme. Since the Michaelis complex did not saturate with the used substrate concentrations, the kinetics of formation of the alkylated enzyme are described as a one-step process with the rate constant k_2/K_S (Scheme 3).

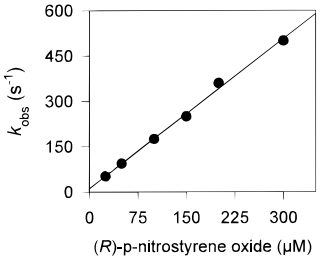

FIGURE 8: Pre-steady-state kinetics of wild-type epoxide hydrolase with (*R*)-PNSO. Multiple-turnover experiments were performed on a stopped-flow fluorescence apparatus with 1 μM enzyme and 25−300 μM substrate at 30 °C in TE buffer. The recorded traces were fitted to a single exponential, and the resulting k_{obs} values were plotted as a function of the (*R*)-PNSO concentration. The solid line shows a fit of the data with Scheme 3 and the data in Table 3.

Scheme 2

$$E + S \underset{}{\overset{K_S}{\rightleftharpoons}} [ES] \underset{k_{-2}}{\overset{k_2}{\rightleftharpoons}} E\text{-}S \xrightarrow{k_3} E + P$$

Scheme 3

$$E + S \underset{k_{-2}}{\overset{k_2/K_S}{\rightleftharpoons}} E\text{-}S \xrightarrow{k_3} E + P$$

The data of Figure 8 were fitted with the analytical solution of Scheme 3 using the equation $k_{obs} = (k_2/K_S)[S] + k_{-2} + k_3$ (*11*, *17*). The K_m value of wild-type enzyme for (*R*)-PNSO followed directly from the fit, since it is defined as the *y*-axis intercept devided by the slope, yielding the equation $K_m = K_s(k_{-2} + k_3)/k_2$. This resulted in a K_m value of 7 μM, which

Table 4: Inhibition Constants of Phenylacetamide on the Activity of Wild-Type Epoxide Hydrolase

inhibitor	inhibition constant (mM)
phenylacetamide	0.03
phenoxyacetamide	0.6
benzamide	1.1
phenylcarbamate	1.6
p-nitrobenzamide	2
p-chlorobenzamide	3
chloroacetamide	3.5
ureum	5
acetamide	37

is close to the experimentally determined value (Table 1). Since k_{cat} is defined as k_3 in this model, a solution could be found for the kinetic constants (Table 3). Only lower limits could be set for K_S and k_2. Due to the fast alkylation rate of the enzyme, the K_m of 7 μM is much lower than the lower limit of K_S. The formation of the alkyl-enzyme intermediate was found to be reversible, and the hydrolysis of this intermediate was rate-limiting.

Multiple-turnover experiments with (*R*)-PNSO and the Y215F and Y152F mutants did not result in observable quenching of the protein fluorescence. The maximum solubility of 1 mM (*R*)-PNSO in combination with the K_m values of these mutants, which were close to or higher than the maximum solubility, causes the quenching to be too faint to be useful.

Glutamine 134. Gln134 takes a prominent position in the X-ray structure of epoxide hydrolase by blocking the proposed active site cavity (Figure 1). To have a better understanding of the function of Gln134 and to explain its position in the active site of the X-ray structure of epoxide hydrolase, it was mutated to Ala. The Q134A mutant was purified, and the steady-state kinetic parameters were determined (Table 1). The data clearly showed that mutation of Gln134 to Ala had no dramatic effect on catalysis, since the K_m values were only moderately raised and the k_{cat} values were still high, although they have decreased 3-fold. Clearly, Gln134 does not have a catalytic function in epoxide hydrolase.

Amide Inhibitors. The binding of the Gln134 side chain in the crystal structure of epoxide hydrolase between the side chains of Tyr152, Tyr215, and the nucleophile Asp107 suggests that molecules with an unsubstituted amide function may also bind at this position. To test this hypothesis, the inhibitory effect of a selection of primary amides on the conversion of (*R*)-PNSO was determined (Table 4). All tested amides caused competitive inhibition of the conversion of (*R*)-PNSO by wild-type enzyme. Phenylacetamide was the best inhibitor with a K_i of 30 μM. The high K_i value of the wild-type enzyme for acetamide indicates that the additional phenyl group of phenylacetamide contributes significantly to the binding efficiency.

The inhibitor phenylacetamide was used to determine the binding characteristics of the mutant epoxide hydrolases (Table 5). All tested mutant enzymes had lower affinities for phenylacetamide than wild-type enzyme. The K_i values of the tyrosine mutants for phenylacetamide were determined from the effect on the k_{cat}/K_m ratio of (*R*)-PNSO, and since wild-type enzyme and the Gln134Ala mutant displayed competitive inhibition, it was also assumed for the tyrosine mutants. The Y152F mutant, which had the highest K_m value for (*R*)-SO, showed the strongest reduction in affinity for phenylacetamide. The substrate binding constant of the Y215F mutant was 3 times lower than the binding constant of the Y215A mutant (Table 3), but the inhibition constant of phenylacetamide was 3 times higher for the Y215F mutant than for the Y215A mutant (Table 5). Thus, there is no direct relationship between the binding constants of phenylacetamide and (*R*)-SO for the Tyr215 mutants, indicating that phenylacetamide is not a simple substrate analogue. The extent of accumulation of the first covalent intermediate in the conversion of (*R*)-SO is higher for the Y215A mutant than for the Y215F mutant, and this relates better to the inhibition constants of these mutants for phenylacetamide. Therefore, it seems that phenylacetamide is a transition-state analogue.

Table 5: Inhibition Constants of Wild-Type and Mutant Enzymes with Phenylacetamide

enzyme	inhibitor constant (mM)
wild type	0.03
Y152F	2.0
Y215F	0.75
Y215A	0.27
Q134A	0.20

DISCUSSION

Role of Tyr152 and Tyr215 in Catalysis. The recently obtained X-ray structure of epoxide hydrolase from *Agrobacterium radiobacter* AD1 allowed the identification of two tyrosine residues from the cap domain region that play an important role in catalysis (*9*, *14*). In this paper, we show that mutation of Tyr152 to Phe and Tyr215 to Phe and Ala resulted in stable mutant enzymes which were seriously affected in the alkylation half-reaction, as was clear from the changed kinetic properties of the tyrosine mutants compared to wild-type enzyme. The K_m values of the tyrosine mutants for the (*R*)-enantiomers of SO and PNSO are 100−1000-fold higher than the K_m values of wild-type enzyme, whereas the k_{cat} values of the mutants for these substrates are only slighty reduced. The hydrolysis rates of the covalent intermediate of wild-type enzyme with (*R*)-SO and (*R*)-PNSO are rate-determining, and since only the K_m values changed dramatically in the mutant enzymes, the major kinetic difference between wild-type and mutant enzymes is expected in the substrate binding step and in the alkylation reaction. This postulation was made earlier on basis of the steady-state kinetics (*14*) and is confirmed in this study by the pre-steady-state kinetics of the Y215F and Y215A mutants for (*R*)-SO.

Removal of Tyr152 or Tyr215 from the active site reduces but does not completely abolish enzyme activity. When both tyrosines are mutated to Phe, the resulting double mutant is virtually inactive, while the structural integrity has not changed. Thus, the presence of one tyrosine residue in the active site of epoxide hydrolase is essential for enzyme activity, but two tyrosines are needed for the high substrate affinity that is displayed by the wild-type enzyme.

The X-ray structure of epoxide hydrolase shows that Tyr152 and Tyr215 form perfect hydrogen bonds with the carbonylic oxygen of Gln134 in the active site (Figure 1). Similar hydrogen bonding of the epoxide oxygen is expected

between the phenolic groups of Tyr152 and Tyr215 (*9*). Indeed, mutation of Tyr152 or Tyr215 resulted in a weakened Michaelis complex, as was evident from the increased binding constants. The K_S of the Y215F and Y215A mutants for (*R*)-SO increased 15- and 40-fold, respectively, compared to wild-type enzyme. No individual rate constants could be obtained for the conversion of (*R*)-SO by the Y152F mutant, but the high K_m value for (*R*)-SO indicated that the K_S was increased at least 40-fold compared to wild-type enzyme, since the K_m value sets the lower limit for the K_S value when the reaction mechanism contains at least three reaction steps (*19*). The 10−70-fold increase of the inhibition constants of the mutant enzymes for phenylacetamide shows that binding is impaired. Thus, removal of one potential hydrogen bond leads to less efficient binding of substrate or inhibitor in the active site of epoxide hydrolase, and as a result, the K_m values for various substrates are increased. Besides the formation of hydrogen bonds to the oxirane ring by the two tyrosine residues, the aromatic moiety of the substrate or inhibitor also contributes significantly to the binding efficiency. The inhibition constants of acetamide and phenylacetamide demonstrate that an additional phenyl group results in a 1000-fold lower inhibition constant for wild-type enzyme.

The second step in the catalytic cycle of epoxide hydrolase is the reversible formation of the covalent intermediate, and this step has changed considerably in the Tyr215 mutants. The wild-type enzyme shows extensive accumulation of the covalent intermediate during turnover of (*R*)-PNSO and (*R*)-SO, since the alkylation rates, which are on the order of 1000 s^{-1}, are much faster than the subsequent steps. The alkylation reaction is reversible in the wild-type enzyme, but since the dealkylation rate is about 30-fold lower than the alkylation rate, the equilibrium lies toward the alkyl-enzyme intermediate (*11*). The high stability of the alkyl-enzyme intermediate in wild-type enzyme indicates that the intermediate is efficiently kept protonated by the two tyrosine residues. The pK_a of the proton-donating tyrosine in wild-type epoxide hydrolase was estimated from enzyme inactivation studies and found to be 10.9, which is lower than the pK_a of an aliphatic alcohol (*20*). We propose that the emerging oxyanion is directly protonated by one of the tyrosine residues upon ring opening. Further indications that proton transfer is a concerted reaction with the formation of the alkyl-enzyme intermediate come from the observation that quenching of the protein fluorescence occurs solely in this intermediate state. The presence of a tyrosinate in the alkyl-enzyme intermediate is thought to be responsible for the decrease in fluorescence, as will be discussed later.

The Y215F and Y215A mutants showed only minor accumulation of the first covalent intermediate upon reaction with (*R*)-SO, as can be observed from the small initial fluorescence decrease. The alkylation rates of the Tyr215 mutants with (*R*)-SO are about 20-fold lower than the alkylation rate of wild-type enzyme, but they have not become rate-limiting. The dealkylation rate has increased for the Y215F mutant compared to wild-type enzyme and is even 2.5 times faster than the alkylation rate, resulting in a shift of the equilibrium from the covalent intermediate state toward the Michaelis complex. The Y215A mutant has a slightly lower dealkylation rate than wild-type enzyme, but it is only 3 times lower than the alkylation rate, indicating that the covalent intermediate is not nearly as stable as in wild-type enzyme. The decreased alkylation rates indicate that Tyr215 plays an important role in the activation of substrate in the transition state. The relative fast dealkylation rates for the Tyr215 mutants show that the alkyl-enzyme is not stable, probably since the remaining Tyr152 cannot efficiently maintain a protonated covalent intermediate.

The steady-state kinetic parameters of the Y152F mutant for (*R*)-SO were of the same order of magnitude as those of the Tyr215 mutants, and, therefore, similar alkylation and dealkylation rates are also expected for the Y152F mutant. The observation that a single tyrosine residue still protonates but yields an unstable alkyl-enzyme intermediate suggests that the second tyrosine in wild-type enzyme is needed for stabilization of the negative charge on the neighboring tyrosinate by hydrogen bond formation. This may also explain that the sequence alignment in Figure 2 shows a His residue instead of a Tyr residue in the sequence of the epoxide hydrolase from *Corynebacterium* sp. at the position that matches Tyr152, while a tyrosine is conserved at the position equivalent to Tyr215. A histidine is probably also capable of stabilizing the tyrosinate that is formed when the epoxide ring is cleaved in this enzyme. It was shown for human aldose reductase that mutation of the proton-donating Tyr48 to His resulted in a mutant enzyme that still showed some enzyme activity while the Y48F mutant was inactive (*21*). This indicates that a His residue can serve as a substitute for Tyr to some extent.

The results clearly indicate the involvement of Tyr152 and Tyr215 in the alkylation reaction, allowing more insight into the transition state of the alkylation reaction. Indications about the nature of the transition state come from studies on different epoxide hydrolases. The half-life of the enzyme−inhibitor complex of mouse and human soluble epoxide hydrolase with various para-substituted chalcone oxides gave a Hammett correlation that indicated the development of a positive charge at the reactive center in the early transition state structure of the epoxide opening (*22*). The conversion of various para-substituted styrene oxides by an unidentified soluble epoxide hydrolase from *Syncephalastrum racemosum* gave indications about the importance of electrophilic activition of the epoxide (*13*). Although it has not been directly established which chemical step is rate-determining, it may well be the alkylation reaction which is influenced. In that case, these studies indicate that the transition state of the activated substrate of the mentioned epoxide hydrolases has a partially opened epoxide ring. These experiments were performed with other epoxide hydrolases and different substrates, but sequence alignments indicate that all epoxide hydrolases possess at least one tyrosine residue in the active site. In fact, the recently solved structure of murine soluble epoxide hydrolase shows the presence of Tyr381 and Tyr465 in the active site in close proximity of the nucleophilic Asp333 (*23*). These Tyr residues are aligned with the Tyr residues 152 and 215 of the epoxide hydrolase that is characterized in this study (Figure 2). This strongly indicates that epoxide hydrolases in general need two Tyr residues for catalytic activity and high substrate affinity.

A proposed model for the transition state of activated substrate is shown in Figure 9. Upon substrate binding, hydrogen bonds are formed between the epoxide ring and the two tyrosine residues which result in the polarization of the C−O bond that has to be cleaved. The epoxide oxygen

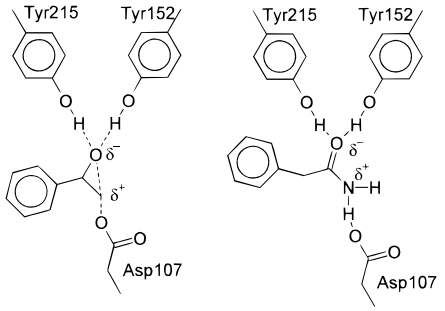

FIGURE 9: Comparison of the transition state of the alkylation reaction and the binding of the reversible inhibitor phenylacetamide. The left structure shows the proposed transition state of activated substrate in the active site of epoxide hydrolase by the interaction of the hydroxyl groups of Tyr152 and Tyr215 with the epoxide ring of styrene oxide. The right structure shows the binding of the reversible inhibitor phenylacetamide between the two tyrosines and the nucleophile Asp107 in analogy with the observed position of Gln134 in the X-ray structure of epoxide hydrolase.

atom is slightly negatively charged, and the primary carbon atom becomes slightly positively charged, which facilitates nucleophilic attack of the negatively charged nucleophile Asp107 at this carbon atom. A negative charge emerges on the oxirane oxygen as a result of the progressive formation of a covalent bond between the primary carbon atom of substrate and the carboxylic side chain of Asp107. The newly formed oxyanion is stabilized by dislocation of the negative charge to one of the tyrosines by transferring a proton. This general acid catalysis is impaired in the Tyr mutants as is evident from the low alkylation rates, but the presence of one tyrosine residue is still sufficient to activate the substrate and to stabilize the negatively charged oxygen atom in the transition state to some extent. An alternative mechanism in which the oxirane ring is first protonated by the tyrosine residues, resulting in ring opening and the formation of a carbocation on the substrate, is not considered very likely. A secondary carbocation is more stable than a primary carbocation, and as a consequence, the formation of an ester would be preferred at the secondary carbon atom of the epoxide ring. This does not agree with the observation that this epoxide hydrolase attacks the least-hindered carbon atom (*8*, *24*).

The second part of the reaction mechanism, the hydrolysis half-reaction, is less affected by mutation of one of the tyrosine residues. The unimolecular isomerization that follows the formation of the covalent intermediate in the reaction sequence of wild-type for (*R*)-SO is slightly affected by the mutation of Tyr215 to Phe and Ala, resulting in 2- and 5-fold reduction of the rate constant, respectively. The nature of this isomerization step is unclear, and it is not known if Tyr215 or Tyr152 is involved in this step. The unimolecular isomerization was accompanied by a fluorescence increase. Recently, we proposed that a protonation event, possibly reprotonation of the proton donor during a conformational change, may cause this increase (*11*). Indeed, protonation of the tyrosinate in the covalent state would annihilate the source of quenching, as will be discussed later. The conversion of (*R*)-PNSO and (*S*)-SO by wild-type enzyme (*11*) did not involve this unimolecular isomerization step, indicating that it is specific for the conversion of (*R*)-SO.

The hydrolysis of the covalent intermediate, which is the last and slowest reaction step in the catalytic cycle, is not lowered in the Tyr215 mutants. In fact, the hydrolysis rate has even increased 2-fold for the Y215F mutant with (*R*)-SO. The precise positioning of the catalytic triad residues is critical for efficient hydrolysis, and since the hydrolysis rates are not affected in the mutant enzymes, the mutation of a single tyrosine residue has apparently no disrupting effect on the structural integrity of the active site. This is also shown by the circular dichroism spectra of the mutant enzymes, which were identical to that of wild-type enzyme. The hydrolysis rates of the Tyr215 mutants for (*R*)-SO are higher than the k_{cat} values of these enzymes for (*R*)-SO, while the hydrolysis rate in wild-type enzyme is almost identical to the k_{cat} value. Although the lowered rate constants of the alkylation half-reaction of the Tyr215 mutants for (*R*)-SO have not become really rate-limiting, they are responsible for the decrease in k_{cat}.

Origin of Intrinsic Protein Fluorescence Quenching. The pre-steady-state decrease of the intrinsic protein fluorescence on addition of substrate is associated with the formation of the covalent intermediate and not with substrate binding (*11*). The same observation was made for rat microsomal epoxide hydrolase (*12*). The binding of the inhibitor phenylacetamide, which bears some structural resemblance to SO, has also no effect on the protein fluorescence. Since quenching is only associated with the alkyl-enzyme, it is likely that the generation of the negative charge on either the substrate or a tyrosine is causing the observed decrease in fluorescence. Protonation of the alkyl-enzyme still occurs in the single tyrosine mutants, and the pre-steady-state experiments show that quenching of the protein fluorescence is still visible.

The X-ray structure of epoxide hydrolase shows that two tryptophan residues, Trp38 and Trp183, are situated close to residues Tyr152 and Tyr215 and line the active site. In haloalkane dehalogenase, an enzyme that is structurally related to epoxide hydrolases and also has an aspartate as nucleophile, the binding of 1,2-dichloroethane between the side chains of Trp125 and Trp175 results in collisional quenching of the protein fluorescence (*25*, *26*). Since the binding of substrate does not affect the fluorescence of epoxide hydrolase, the observed decrease in fluorescence associated with the alkyl-enzyme intermediate must be caused by a different mechanism. Furthermore, the side chains of tryptophan residues 38 and 183, which line the active site of epoxide hydrolase, are only 3.7 Å apart, leaving ample room for substrate to bind between (Figure 1). The formation of a protonated 2-hydroxy-alkyl-enzyme is associated with the generation of a tyrosinate, and tyrosinates are known to be excellent quenchers of the tryptophan fluorescence by a mechanism that concerns resonance energy transfer from the tryptophan to the tyrosinate (*27*−*29*). Laws and Shore (*28*) reported that the deprotonated Tyr286 of liver alcohol dehydrogenase quenches the fluorescence of Trp314 even over a distance of 17 Å, as long as the orientation of the tyrosinate and the tryptophan is optimal. Although there are two tryptophan residues that line the active site of epoxide hydrolase, no direct contact is needed between the covalently bound substrate and the tryptophan residues in order to obtain quenching. Sequence alignments of different epoxide hydrolases indicated that tyrosine residues are conserved. Since at least one tyrosine residue is conserved in rat microsomal

epoxide hydrolase (Tyr374), the observed quenching with glycidyl-4-nitrobenzoate probably also results from the formation of a tyrosinate in the alkylation reaction.

Glutamine 134. The amide side chain of Gln134 is bound in the active site at the position where substrate is supposed to bind. The mutation of Gln134 to Ala shows that there are only minor changes of the steady-state kinetics compared to wild-type enzyme, indicating that Gln134 is not essential for catalysis. Substrate analogues with an amide function also bind in the active site as was evident from the inhibition experiments, indicating that the active site has an affinity for amide groups. Nardini et al. (*9*) postulated that Gln134 was only present in the active site due to a distortion of the structure by crystal contacts. The loop containing the acid residue of the catalytic triad, Asp246, which was identified by site-directed mutagenesis, was dislocated from the active site to the solvent, allowing the side chain of Gln134 to move into the active site. Remodeling of the structure to its supposed active conformation positions Gln134 close to the surface of the enzyme (*9*). This is confirmed by the Q134A mutant, which shows only small perturbations in the steady-state kinetics compared to wild-type enzyme. Furthermore, sequence alignments show that Gln134 is not conserved in any of the other epoxide hydrolase sequences, indicating that Gln134 does not serve a function in catalysis. Also the recently solved structure from murine soluble epoxide hydrolase shows that Asp363, which is aligned with Gln134, is not present near the active site.

Amide Inhibitors. The pre-steady-state kinetics of the Y215F and Y215A mutants for (*R*)-SO and the inhibition constants of phenylacetamide for these mutant enzymes suggested that unsubstituted amides behaved more like a transition state analogue then as a substrate analogue. In the transition state of the alkylation reaction, the epoxide ring is partially opened, and the oxygen−carbon bond that has to break is polarized. The geometry of an amide group may resemble the transition state of the alkylation half-reaction, and the amide may also undergo some charge redistribution if the carbonyl oxygen atom is hydrogen-bonded to the tyrosines and if the nitrogen atom mimics the primary carbon atom (Figure 9). The charge redistribution in the amide function is a result of the different resonance structures and may be induced by hydrogen bonding. The reduced binding of phenylacetamide to the Tyr mutants seems to reflect the weakened stabilization of the activated substrate in the transition state during ring opening.

Several amides were found to be reversible inhibitors with inhibition constants in the micromolar range. Phenylacetamide, which has a binding constant of 30 μM, binds even better to epoxide hydrolase than the model substrate (*R*)-SO, which has a binding constant of 90 μM. Unsubstituted amides, such as valpromide, which is the amide derivative of the antiepileptic drug valproate, are described in the literature as inhibitors of human microsomal and soluble epoxide hydrolase (*30*−*32*). Long-chain aliphatic amides were also found to be good inhibitors. The type of inhibition is not mentioned in these cases, but the results in this study indicate that amides may act as competitive inhibitors of epoxide hydrolases. Several urea derivatives and substituted amides were recently found to act as competitive inhibitors of mouse soluble epoxide hydrolase with binding affinities in the nanomolar range (*33*). These observations indicate that amides are general competitive inhibitors of epoxide hydrolases, which may be due to conserved active site geometry.

REFERENCES

1. Beetham, J. K., Grant, D., Arand, M., Garbarino, J., Kiyosue, T., Pinot, F., Oesch, F., Belknap, W. R., Shinozaki, K., and Hammock, B. D. (1995) *DNA Cell Biol. 14*, 61−71.
2. Rink, R., Fennema, M., Smids, M., Dehmel, U., and Janssen, D. B. (1997) *J. Biol. Chem. 272*, 14650−14657.
3. Misawa, E., Chan Kwo Chion, C. K. C., Archer, I. V., Woodland, M. P., Zhou, N.-Y., Carter, S. F., Widdowson, D. A., and Leak, D. J. (1998) *Eur. J. Biochem. 253*, 173−183.
4. Debernard, S., Morisseau, C., Severson, T. F., Feng, L., Wojtasek, H., Prestwich, G. D., and Hammock, B. D. (1998) *Insect Biochem. Mol. Biol. 28*, 409−419.
5. Armstrong, R. N. (1987) *CRC Crit. Rev. Biochem. 22*, 39−88.
6. Archer, I. V. J. (1997) *Tetrahedron 53*, 15617−15662.
7. Archelas, A., and Furstoss, R. (1997) *Annu. Rev. Microbiol. 51*, 491−525.
8. Lutje Spelberg, J. H., Rink, R., Kellogg, R. M., and Janssen, D. B. (1998) *Tetrahedron: Asymmetry 9*, 459−466.
9. Nardini, M., Ridder, I. S., Rozeboom, H. J., Kalk, K. H., Rink, R., Janssen, D. B., and Dijkstra, B. W. (1999) *J. Biol. Chem. 274*, 14579−14586.
10. Ollis, D. L., Cheah, E., Cygler, M., Dijkstra, B. W., Frolow, F., Franken, S. M., Harel, M., Remington, S. J., Silman, I., Schrag, J., Sussman, J. L., Verschueren, K. H. G., and Goldman, A. (1992) *Protein Eng. 5*, 197−211.
11. Rink, R., and Janssen, D. B. (1998) *Biochemistry 37*, 18119−18127.
12. Tzeng, H.-F., Laughlin, L. T., Lin, S., and Armstrong, R. M. (1996) *J. Am. Chem. Soc. 118*, 9436−9437.
13. Moussou, P., Archelas, A., Baratti, J., and Furstoss, R. (1998) *J. Org. Chem. 63*, 3532−3537.
14. Rink, R., Lutje Spelberg, J. H., Pieters, R., Kingma, J., Nardini, M., Kellog, R. M., Dijkstra, B. W., and Janssen, D. B. (1999) *J. Am. Chem. Soc. 121*, 7417−7418.
15. Westkaemper, R. B., and Hanzlik, R. P. (1981) *Arch. Biochem. Biophys. 208*, 195−204.
16. Kunkel, T. A. (1985) *Proc. Natl. Acad. Sci. U.S.A. 82*, 488−492.
17. Johnson, K. A. (1992) *Enzymes (3rd Ed.) 20*, 1−61.
18. Gutfreund, H. (1995) *Kinetics for the Life Sciences: Reporters, Transmitters and Catalysts*, Cambridge University Press, Cambridge, U.K.
19. Fersht, A. R. (1985) *Enzyme Structure and Mechanism*, 2nd ed., W. H. Freeman, New York.
20. Maskill, H. (1985) *The physical basis of organic chemistry*, p 166, Oxford University Press, New York.
21. Bohren, K. M., Grimshaw, C. E., Lai, C.-J., Harrison, D. H., Ringe, D., Petsko, G. A., and Gabbay, K. H. (1994) *Biochemistry 33*, 2021−2032.
22. Morisseau, C., Du, G., Newman, J. W., and Hammock, B. D. (1998) *Arch. Biochem. Biophys. 356*, 214−228.
23. Argiriadi, M. A., Morisseau, C., Hammock, B. D., and Christianson, D. W. (1999) *Proc. Natl. Acad. Sci. U.S.A. 96*, 10637−10642.
24. Jacobs, M. H. J., van den Wijngaard, A. J., Pentenga, M., and Janssen, D. B. (1991) *Eur. J. Biochem. 202*, 1217−1222.
25. Schanstra, J. P., and Janssen, D. B. (1996) *Biochemistry 35*, 5624−5632.
26. Pries, F., Kingma, J., Pentenga, M., Van Pouderoyen, G., Jeronimus-Stratingh, C. M., Bruins, A. P., and Janssen, D. B. (1994) *Biochemistry 33*, 1242−1247.
27. Ramanchandran, N., and Ghiron, C. A. (1978) *Biochim. Biophys. Acta 532*, 286−293.
28. Laws, W. R., and Shore, J. D. (1978) *J. Biol. Chem. 253*, 8593−8597.
29. Jang, D.-J., and El-Sayed, M. A. (1989) *Proc. Natl. Acad. Sci. U.S.A. 86*, 5815−5819.

30. Pacifici, G. M., and Rane, A. (1987) *Pharmacol. Toxicol. 60*, 237−238.
31. Kerr, B. M., Rettie, A. E., Eddy, A. C., Loiseau, P., Guyot, M., Wilensky, A. J., and Levy, R. H. (1989) *Clin. Pharmacol. Ther. 46*, 82−93.
32. Kerr, B. M., and Levy, R. H. (1990) *Drug Metab. Dispos. 18*, 540−542.
33. Morisseau, C., Goodrow, M. H., Dowdy, D., Zheng, J., Greene, J. F., Sanborn, J. R., and Hammock, B. D. (1999) *Proc. Natl. Acad. Sci. U.S.A. 96*, 8849−8854.

BI9922392